Author Manuscript

Author Manuscript

Author Manuscript

Author Manuscript

HHS Public Access

Author manuscript

Inorg Chem. Author manuscript; available in PMC 2017 October 17.

Published in final edited form as:

Inorg Chem. 2016 October 17; 55(20): 10800–10809. doi:10.1021/acs.inorgchem.6b02109.

High-Valent Manganese-Oxo Valence Tautomers and the Influence of Lewis/Brönsted Acids on C−H Bond Cleavage

Regina A. Baglia[†], **Courtney M. Krest**[‡], **Tzuhsiung Yang**[†,§], **Pannee Leeladee**[†,‖], and **David P. Goldberg**[*,†]

[†]Department of Chemistry, The Johns Hopkins University, 3400 North Charles Street, Baltimore, Maryland 21218, United States

[‡]Stanford Synchrotron Radiation Lightsource, SLAC National Accelerator Laboratory, Menlo Park, California 94025, United States

Abstract

The addition of Lewis or Brönsted acids (LA = $Zn(OTf)_2$, $B(C_6F_5)_3$, $HBAr^F$, TFA) to the high-valent manganese—oxo complex $Mn^V(O)(TBP_8Cz)$ results in the stabilization of a valence tautomer $Mn^{IV}(O\text{-}LA)(TBP_8Cz^{\bullet+})$. The Zn^{II} and $B(C_6F_5)_3$ complexes were characterized by manganese K-edge X-ray absorption spectroscopy (XAS). The position of the edge energies and the intensities of the pre-edge (1s to 3d) peaks confirm that the Mn ion is in the +4 oxidation state. Fitting of the extended X-ray absorption fine structure (EXAFS) region reveals 4 N/O ligands at $Mn-N_{ave}$ = 1.89 Å and a fifth N/O ligand at 1.61 Å, corresponding to the terminal oxo ligand. This Mn−O bond length is elongated compared to the $Mn^V(O)$ starting material (Mn−O = 1.55 Å). The reactivity of $Mn^{IV}(O\text{-}LA)(TBP_8Cz^{-+})$ toward C−H substrates was examined, and it was found that $H^{\bullet}$ abstraction from C−H bonds occurs in a 1:1 stoichiometry, giving a Mn^{IV} complex and the dehydrogenated organic product. The rates of C−H cleavage are accelerated for the $Mn^{IV}(O\text{-}LA)(TBP_8Cz^{\bullet+})$ valence tautomer as compared to the $Mn^V(O)$ valence tautomer when LA = Zn^{II}, $B(C_6F_5)_3$, and $HBAr^F$, whereas for LA = TFA, the C−H cleavage rate is slightly slower than when compared to $Mn^V(O)$. A large, nonclassical kinetic isotope effect of k_H/k_D = 25–27 was observed for LA = $B(C_6F_5)_3$ and $HBAr^F$, indicating that H-atom transfer (HAT) is the rate-limiting step in the C−H cleavage reaction and implicating a potential tunneling mechanism for HAT. The reactivity of $Mn^{IV}(O\text{-}LA)(TBP_8Cz^{\bullet+})$ toward C−H bonds depends on the strength of the Lewis acid. The HAT reactivity is compared with the analogous corrole complex $Mn^{IV}(O-H)(tpfc^{\bullet+})$ recently reported.

[*]**Corresponding Author:** dpg@jhu.edu.

[§]**Present Addresses**

T.Y.: Department of Chemistry, University of Wisconsin—Madison, 1101 University Avenue, Madison, Wisconsin 53706, United States.

‖ P.L.: Department of Chemistry, Faculty of Science Chulalongkorn University, Phayathai Road, Pathumwan Bangkok 10330, Thailand.

ASSOCIATED CONTENT

Supporting Information

The Supporting Information is available free of charge on the ACS Publications website at DOI: 10.1021/acs.inorg-chem.6b02109.

UV−vis kinetics studies, $^{31}P\{^1H\}$ NMR, EPR spectra, and DFT calculations (PDF)

The authors declare no competing financial interest.

Author Manuscript Author Manuscript Author Manuscript Author Manuscript

Graphical Abstract

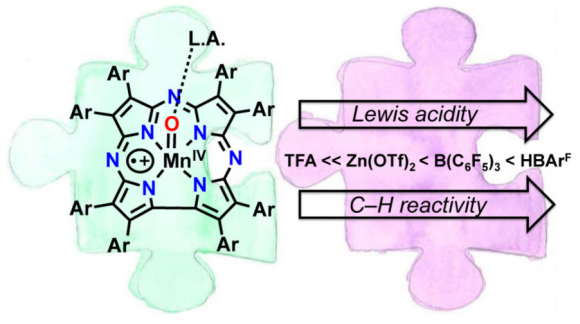

INTRODUCTION

A broad range of heme enzymes rely on high-valent iron-oxo porphyrin intermediates to carry out substrate oxidation.[1–3] The general structure of these species can be divided into $Fe^{IV}(O)(Por^{\bullet+})(X)$ (Compound I (Cpd-I), $Por^{\bullet+}$ = porphyrin π-radical-cation, X = axial ligand) and $Fe^{IV}(O)(por)$ (Compound II (Cpd-II)). Cpd-I can be a potent oxidant and is capable of cleaving C−H bonds with bond strengths up to ~95 kcal/mol in Cytochrome P450. Cpd-II is usually considered to be a weaker oxidant than Cpd-I, in part because Cpd-I is at the formally higher oxidation level of Fe^{V}. The redox-active nature of the porphyrin ligand allows access to such formally high oxidation states because of the porphyrin's ability to delocalize some of the positive charge on the aromatic *π* system. The delocalization can be viewed in the extreme case as an intramolecular electron transfer from the porphyrin ligand to the oxidized metal center, resulting in a "valence tautomer" with a one-electron-reduced metal center and a π-based radical on the ring. There was significant debate regarding which valence tautomer best described Cpd-I in Cyt-P450 until recently, when definitive spectroscopic evidence showed that this species corresponded to the $Fe^{IV}(O)$ (π-radical-cation) tautomer.[1] However, the requirements for stabilizing one valence tautomer over the other in high-valent metalloporphyrins and their relative reactivities remains poorly understood.

In synthetic porphyrin systems, valence tautomerism has been induced by chemical or nonchemical (temperature, irradiation) changes.[4–6] However, there are few examples of metal-oxo complexes in which both valence tautomers have been characterized. Our group showed previously that treatment of $Mn^{V}(O)(TBP_8Cz)$ (TBP_8Cz = octakis(*p-tert*-butylphenyl)corrolazinato^{3-}) with metallic and nonmetallic Lewis and Brönsted acids (LA = $Zn(OTf)_2$, $B(C_6F_5)_3$, H^+) (OTf = trifluoromethylsulfonate^{1-}) led to stabilization of the valence tautomer $Mn^{IV}(O\text{-}LA)(TBP_8Cz^{\bullet+})$ with an Mn^{IV} ion coupled to a corrolazine π-cation-radical and the Lewis/Brönsted acid bound to the terminal oxo ligand.[7–10] The $Mn^{IV}(O\text{-}LA)(TBP_8Cz^{\bullet+})$ complexes exhibited significantly enhanced reactivity toward O-H bond cleavage with phenol derivatives in comparison to the closed-shell $Mn^{V}(O)$-(TBP_8Cz). In contrast, dramatically decreased rates of oxygen atom transfer (OAT) to triarylphosphines were observed for $Mn^{IV}(O\text{-}LA)(TBP_8Cz^{\bullet+})$ as compared to the $Mn^{V}(O)$ tautomer. Acid-dependent valence tautomerism was observed when trifluoroacetic acid (TFA) was added to

Author Manuscript Author Manuscript Author Manuscript Author Manuscript

$Fe^{IV}(O)$-$(TPFP^{\bullet+})(L)$ (TPFP = 5,10,15,20-tetrakis(pentafluorophenyl)-porphyrinato^{2-}), resulting in the formation of the isoporphyrin complex $Fe^{III}(TPFP^{2+})(L)_2$.[11] Addition of chloride ion to the isoporphyrin complex allowed for chlorination of aromatic compounds and olefins. More recently, reversible valence tautomerism was implicated for oxo−ferryl porphyrins by stopped-flow UV−vis spectroscopy, where $Fe^{IV}(O)(por)$ was present at high pH but could be converted to $Fe^{III}(OH_2)$-$(por^{\bullet+})$ at low pH.[12]

In Mn(salen) systems, addition of 1 equiv of hydroxide to $Mn^{III}(OH_2)(salen^{\bullet+})$ resulted in the formation of the valence tautomer $Mn^{IV}(OH)$(salen). Further deprotonation of this complex gave the $Mn^{IV}(O)$(salen) complex, which was the most reactive complex in this series in both HAT and OAT reactions.[13] In 2015, Abu-Omar showed that addition of TFA to $Mn^{V}(O)$(tpfc) (tpfc = 5,10,15-tris(pentafluorophenyl)-corrolato^{3-}) resulted in formation of the valence tautomer $Mn^{IV}(OH)(tpfc^{\bullet+})$.[14]

Lewis and Brönsted acids are known to exert a critical influence on the reactivity of metal −oxo and related species. In biological systems, these acids can play important roles in tuning redox potentials and redox reactivity. One example is the nonredox active Ca^{2+} ion bound to the Mn cluster of the oxygen-evolving complex (OEC) in Photosystem II.[15–17] Possible intermediates during water oxidation by the OEC are high-valent $Mn^{IV}(O)/Mn^{V}(O)$ species, and the role of the Ca^{2+} ion in this process remains poorly understood. Addition of redox inactive metal ions to manganese−oxo cluster complexes allowed for modulation of the reduction potentials of these compounds.[16] The addition of Lewis/Brönsted acids (e.g., Sc^{3+}, HOTf) has been found to enhance electron transfer (ET), OAT, and PCET (PCET = proton-coupled electron transfer) rates of nonheme $Fe^{IV}(O)$ complexes.[18] Addition of triflic acid and $Sc(OTf)_3$ to nonheme $Mn^{IV}(O)$ complexes was found to accelerate ET and OAT rates but inhibit rates of H-atom abstraction.[19,20] Nonredox active metal ions have also been found to accelerate the rates and improve efficiencies of Mn-mediated catalytic oxidation reactions.[21,22] The rates of O_2 activation in nonheme Mn and Fe complexes were also enhanced in the presence of Lewis acids.[23] In these nonheme systems, however, valence tautomerism did not come into play.

In this work, a series of $Mn^{IV}(O\text{-}LA)(TBP_8Cz^{\bullet+})$ complexes (LA = $Zn(OTf)_2$, $B(C_6F_5)_3$, $HBAr^F$, CF_3CO_2H) is generated and their reactivity toward C−H bond cleavage is assessed. The $Mn^{IV}(O\text{-}LA)(TBP_8Cz^{\bullet+})$ complexes (LA = $Zn(OTf)_2$, $B(C_6F_5)_3$) were characterized by Mn K-edge X-ray absorption spectroscopy (XAS), providing the first structural information for these complexes and yielding key information on both the oxidation state of the Mn and the perturbation of the Mn−O bond length. The reactivity of the $Mn^{IV}(O\text{-}LA)(TBP_8Cz^{\bullet+})$ complexes with a series of C−H substrates of varying C−H bond strengths (BDE(C−H)) was studied. Rate enhancements of C−H cleavage were observed for the Lewis acid complexes compared to the closed-shell $Mn^{V}(O)$ valence tautomer, with the exception of TFA. The magnitude of the rate enhancement depended strongly on the identity of the Lewis acid.

Author Manuscript Author Manuscript Author Manuscript Author Manuscript

RESULTS AND DISCUSSION

Synthesis and Structural Characterization of the Mn^{IV}(O-LA)($TBP_8Cz^{\bullet+}$) Complexes by X-ray Absorption Spectroscopy

Previously, we found that the addition of Lewis/Brönsted acids (Zn^{II}, $B(C_6F_5)_3$, $HBAr^F$, HBF_4) to closed-shell Mn^{V}(O)(TBP_8Cz) resulted in stabilization of the open-shell valence tautomer Mn^{IV}(O-LA)($TBP_8Cz^{\bullet+}$) in solution. Characterization of the latter species was carried out by UV−vis, NMR, and EPR spectroscopies and in the case of $B(C_6F_5)_3$ by ESI-MS, which confirmed the 1:1 nature of the Lewis acid adduct. The spectroscopic data showed that the open-shell Mn^{IV}(O-LA)($TBP_8Cz^{\bullet+}$) complexes were paramagnetic, with an Mn^{IV} ion ferro- or antiferromagnetically coupled to a π-cation-radical on the Cz ring. Valence tautomerization was reversible, with the closed-shell Mn^{V}(O) complex being favored upon addition of the appropriate reagent to sequester the Lewis/Brönsted acid (Scheme 1).

Although the Mn^{IV}(O-LA)($TBP_8Cz^{\bullet+}$) complexes are stable at 23 °C in dilute solution, attempts to isolate these complexes as solids results in autoreduction to Mn^{III}. Therefore, we sought to obtain structural information on Mn^{IV}(O-LA)($TBP_8Cz^{\bullet+}$) in solution by X-ray absorption spectroscopy (XAS). XAS is incompatible with halogenated solvents because of large background fluorescence from the solvent, and we needed to find an alternative to the previously employed mixed solvent system CH_2Cl_2/CH_3CN.

The Mn^{IV}(O-LA)($TBP_8Cz^{\bullet+}$) complexes were formed in benzonitrile by addition of Lewis acid to Mn^{V}(O)(TBP_8Cz), and the UV—vis spectral changes matched those seen in CH_2Cl_2/CH_3CN. The Mn K-edge X-ray absorption spectra for Mn^{V}(O)(TBP_8Cz) and Mn^{IV}(O-LA)($TBP_8Cz^{\bullet+}$) (LA = Zn^{II}, $B(C_6F_5)_3$) are shown in Figure 1. The XAS data for Mn^{V}(O)(TBP_8Cz) was reported previously[24,25] but was remeasured here for comparison. The energy of the rising Mn K-edge is dependent on both oxidation state and structure. The positions of the rising edge for the Lewis acid adducts are shifted to lower energy relative to Mn^{V}(O)(TBP_8Cz). This shift is consistent with a lowering of the oxidation state on the metal, and the edge energies match well with other Mn^{IV} complexes.[13,26,27] The intensity of the pre-edge peaks for Mn^{IV}(O-LA)($TBP_8Cz^{\bullet+}$) at ~6541.3 eV are significantly lower than the peak seen for Mn^{V}(O)(TBP_8Cz) at 6541.6 eV. The pre-edge peak arises from a 1s-to-3d transition, and a decrease in intensity for this transition is consistent with a lengthening of the Mn−O bond, as can be expected from the binding of a Lewis acid to the terminal oxo ligand. Fitting of the EXAFS data (Figure 1, Table 1) for the Mn^{IV}(O-LA)($TBP_8Cz^{\bullet+}$) complexes gives 4 N/O scatterers at an average distance of 1.89 Å from the Mn, in good agreement with Mn−N bond distances for the pyrrole N atoms characterized by single-crystal X-ray diffraction for Mn^{III} and Mn^{V}(O) corrolazines.[24,28] Best fits of the data also required a fifth N/O scatterer at an average of 1.61 Å from the Mn center, which can be assigned to the terminal oxo group (Table 1). The Mn−O distance is elongated by 0.05 Å compared to the starting Mn^{V}(O) which we reported as 1.56 Å in our previous EXAFS measurements[24] and 0.06 Å elongation compared to the distance determined by X-ray crystallography.[28] This change in bond distance is consistent with that seen for several other high-valent M−oxo−Lewis acid (M = Mn, Re, W) complexes, which show M−O bond

Author Manuscript Author Manuscript Author Manuscript Author Manuscript

elongations upon binding of LA in the range Δ(M–O) = 0.05–0.07 Å.[29–32] For best results, fits included an Mn−C scatterer at an average distance of 2.90 Å and a multiple scattering shell of Mn−N−C and Mn−C−N at 3.12 Å. Fits of the EXAFS data for Mn^{IV}(O-Zn^{II})($TBP_8Cz^{\bullet+}$) were not significantly improved by inclusion of backscattering from the Zn ion. However, it is known that the observation of metal−metal scattering in related dimetallic porphyrin systems such as Fe−L−Cu porphyrins (L = O^{2-}, OH^-) is highly dependent on the Fe−L−Cu angle.[33,34] An angle of ~180° leads to the observation of a strong metal− metal scatterer, while an angle of less than ~150° leads to no obvious metal−metal scatterer seen in the EXAFS spectrum. Density functional theory (DFT) calculations (vide infra) on Mn^{IV}(O-Zn^{II})($TBP_8Cz^{\bullet+}$) suggest an Mn−O−Zn angle of <150°, consistent with the absence of metal-metal scattering in the EXAFS for this complex.

In earlier work we employed DFT calculations to analyze the geometry of Mn^{IV}(O-Zn^{II})($TBP_8Cz^{\bullet+}$).[7] The optimized geometry of this complex exhibited an elongated Mn−O bond distance of 1.74 Å and a Zn−O distance of 1.89 Å. The Mn−O bond length is ~0.1 Å longer than the Mn−O distance found experimentally by EXAFS, and therefore, further calculations were performed in this work. Geometry optimizations were carried out using different functional and basis set combinations, and the geometries were not sensitive to the choice of functional/basis set (see Table S1 in SI). Singlet, triplet, and quintet spin states for Mn^{IV}(O-LA)($TBP_8Cz^{\bullet+}$) (LA = Zn^{II} and $B(C_6F_5)_3$) were all assessed. A calculated Mn−O distance of 1.65−1.66 Å is found for the respective triplet states, corresponding to one unpaired spin on the Mn^{IV} ion and one unpaired spin on the Cz ring ($d_\pi^1 a''^1$ configuration). This distance is reasonably close to the experimentally determined value from EXAFS. The calculated Mn −O distances for the other triplet and quintet states examined were not as good a match with the experimental value. The calculations also suggest that the quintet state ($d_{xy}^1 d_{xz}^1 d_{yz}^1 a''^1$) is the ground state, being ~1–5 kcal/mol in energy below the former triplet state, depending on the functional and basis set. However, DFT is known to have significant difficulty in determining the energy ordering of multiple spin states in transition metal complexes, especially in Mn.[35–38] The singlet states were found to be the highest in energy but did show Mn−O distances close to the XAS value. However, the singlet states are not consistent with the experimentally determined paramagnetic π-cation-radical complexes and can be ruled out. Interestingly, surface scans along the Mn−O distance for the triplet states reveal surfaces that are energetically flat (Tables S8 and S9). The Mn−O distances were varied over 0.1 Å, but the relative energies changed by only ~1 kcal/mol. The surface scans suggest that the Mn −O bond is relatively loose compared to the Mn^V(O) starting material. On the basis of these results, we tentatively assign Mn^{IV}(O-LA)($TBP_8Cz^{\bullet+}$) to the triplet state with a $d_\pi^1 a''^1$ configuration.[39,40]

Reactivity with C−H Bonds

The reactivity of Mn^{IV}(O-LA)($TBP_8Cz^{\bullet+}$) complexes with the C−H substrate xanthene (Xn) (Chart 1) was examined for the series of Lewis acids shown in Table 2. The Mn^{IV}(O-LA) ($TBP_8Cz^{\bullet+}$) complexes with LA = $Zn(OTf)_2$, $B(C_6F_5)_3$, and $HBAr^F$ were characterized previously.[7,8,10] A recent report from Abu-Omar showed that TFA reacts with an Mn^V(O) corrole, Mn^V(O)(tpfc), to stabilize the analogous Mn^{IV}(OH)($tpfc^{\bullet+}$) valence tautomer, and the HAT reactivity of this species was examined with phenol O-H substrates.[14] We included

Author Manuscript Author Manuscript Author Manuscript Author Manuscript

TFA in the current study to provide a direct comparison with the corrole system. The characteristic spectral changes for the valence tautomer Mn^{IV}(O-TFA)-($TBP_8Cz^{\bullet+}$) were observed following the addition of TFA to Mn^{V}(O)(TBP_8Cz) (Figure S12). Addition of Xn to the Mn^{IV}(O-LA)($TBP_8Cz^{\bullet+}$) complexes was carried out in CH_2Cl_2 at 23 °C, and the reaction was monitored by UV-vis. Representative data for the reaction of Mn^{IV}(O-$B(C_6F_5)_3$)-($TBP_8Cz^{\bullet+}$) with Xn is shown in Figure 2a. The features for the Mn complex (419, 789 nm) undergo isosbestic conversion to a new species (443, 727 nm) over 30 min. The final spectrum is indicative of [Mn^{IV}(TBP_8Cz)(OH)].[7,8,41] Similar spectral changes were seen for the other LA complexes. The final reaction mixtures were examined by EPR spectroscopy (X-band, 12 K), and revealed intense spectra typical of a high-spin Mn^{IV} (S = 3/2) ion and were quite similar to the spectra seen for other Mn^{IV} corrolazines (Figures S3 – S4).[8,41] Taken together, the UV−vis and EPR data indicate that the reaction of the open-shell valence tautomer with the C−H bond substrate Xn yields a one electron-reduced Mn^{IV} corrolazine and implicates a single hydrogen atom transfer event.

The rates of reaction of Mn^{IV}(O-LA)($TBP_8Cz^{\bullet+}$) with Xn were obtained from plots of absorbance versus time, which were well fit with a single-exponential expression and gave the pseudo-first-order rate constants (k_{obs}). Measurement of k_{obs} versus [Xn] led to linear plots as shown in Figure 2b, whose slope, when normalized per reactive C−H bond n (n = 2 for Xn), gave the second-order rate constants (k_2') shown in Table 2. These rate constants were compared to the reaction of the closed-shell Mn^{V}(O) valence tautomer in the absence of Lewis acids (Table 2, column 3). As can be seen from the k_{LA}/k_{none} values, there is a significant increase in the rate of C−H cleavage for LA = Zn^{II}, $B(C_6F_5)_3$, $HBAr^F$. Rate enhancements were seen previously for Mn^{IV}(O-LA)($TBP_8Cz^{\bullet+}$) (LA = Zn^{II}, $B(C_6F_5)_3$) in similar HAT reactions with substituted phenol O−H substrates, with the more Lewis-acidic triarylborane giving the more reactive species. We quantified the Lewis acidity of the LAs in Table 2 with the Gutmann-Beckett method in which the ^{31}P NMR chemical shifts of Et_3PO are measured in the presence of the different Lewis acids.[44,45] This method leads to the acceptor numbers (A.N.) shown in Table 2, with the higher A.N. values indicating greater Lewis acidity. As seen in Table 2, the second-order rate constants follow an overall correlation with the A.N. values, although the triarylborane gives a slightly larger k_2' value for the Xn substrate than $HBAr^F$. Interestingly, the only Lewis acid that did not accelerate the C−H cleavage rate was TFA. In the work by Abu-Omar, addition of TFA also slightly decreased the H-atom abstraction rate for the corrole complex, although no other Lewis acids were tested in this study.[14] Our results strongly suggest that the identity of the Lewis acid is critical in determining the HAT reactivity of Mn^{IV}(O-LA)(π-cation-radical) complexes (vide infra).

Examination of two of the Mn^{IV}(O-LA)($TBP_8Cz^{\bullet+}$) species with Xn-d_2 revealed large KIEs (k_H/k_D = 25 for $B(C_6F_5)_3$ (Figure 2b), k_H/k_D = 27 for $HBAr^F$), both well above the classical limit. A KIE for this substrate with Mn^{V}(O)(TBP_8Cz) could not be obtained because of very slow reaction rates and the limited solubility of Xn at high concentrations. Previously a classical KIE = 3.2 was observed for O−H versus O−D cleavage with Mn^{IV}(O-LA)($TBP_8Cz^{\bullet+}$) and 2,4,6-tri-*tert*-butylphenol (2,4,6-TTBP).[8] The KIE values indicate that HAT is the rate-limiting step for both O−H and C−H substrates. The KIEs for C−H cleavage are also much larger than that observed for the axially ligated [Mn^{V}(O)(TBP_8Cz)-(X)]$^-$ (X =

Author Manuscript Author Manuscript Author Manuscript Author Manuscript

anionic donor) (KIE(C−H) = 11) or for O−H cleavage by the 5-coordinate $Mn^{V}(O)(TBP_8Cz)$ (KIE(O−H) = 6).[42,46] The corrole complex ($Mn^{IV}(OH)(tpfc^{\bullet+})$) exhibited a particularly small KIE = 1.3 for HAT with 2,4-di-*tert*-butylphenol.[14] The large nonclassical KIEs for $Mn^{IV}(O\text{-}LA)(TBP_8Cz^{\bullet+})$ with C−H substrate suggests that significant tunneling may be occurring through the HAT barrier. Further work is needed to determine the origin of the wide range in KIEs observed for the different corrolazine and corrole complexes.

The stoichiometry for the oxidation of C−H bond substrates by $Mn^{IV}(O\text{-}LA)(TBP_8Cz^{\bullet+})$ was further examined by product analysis for the reaction with 9,10-dihydroanthracene (DHA) as substrate. DHA reacts with $Mn^{IV}(O\text{-}LA)(TBP_8Cz^{\bullet+})$ in CH_2Cl_2 to give the one-electron-reduced Mn^{IV} product, as seen by UV−vis. Analysis of a bulk reaction for $Mn^{IV}(O\text{-}B(C_6F_5)_3)(TBP_8Cz^{\bullet+})$ plus DHA gave a 65% yield of the expected dehydrogenated anthracene product by GC-FID, following the stoichiometry in Scheme 2. On the basis of this stoichiometry, a mechanism is proposed where the first H-atom abstraction gives DHA radical ($DHA^{\bullet}$), which is then rapidly dehydrogenated by another $Mn^{IV}(O\text{-}LA)(TBP_8Cz^{\bullet+})$ via a second H-atom abstraction. The stoichiometry contrasts that found for the closed-shell $Mn^{V}(O)(TBP_8Cz)$, which functions as a two-electron oxidant and abstracts both H atoms from a single DHA, producing one anthracene molecule per $Mn^{V}(O)$ complex.[42,46] The former stoichiometry also fundamentally differs from the analogous corrole $Mn^{IV}(OH)(tpfc^{\bullet+})$, which acts as a two-electron oxidant with phenol substrates to give 2 equiv of phenoxyl radical and 1 equiv of Mn^{III} corrole.[14]

The most reactive species with Xn is $Mn^{IV}(O\text{-}B(C_6F_5)_3)\text{-}(TBP_8Cz^{\bullet+})$, and therefore, we examined the reaction kinetics of this species with the additional C−H substrates $AcrH_2$, DHA, and CHD (Chart 1) to gain further insight into the nature of the HAT reactions and their dependence on substrate C−H bond strength.[47] Similar reaction conditions were used as compared to Xn, and good pseudo-first-order kinetics were observed by UV−vis, showing conversion of $Mn^{IV}(O\text{-}B(C_6F_5)_3)(TBP_8Cz^{\bullet+})$ into the one-electron-reduced Mn^{IV} product for all substrates except the $AcrH_2$, which gives an Mn^{III} product. However, $AcrH_2$ is well known to act as a hydride donor by initial $H^{\bullet}$ abstraction followed by fast electron transfer.[41] Normalized second-order rate constants (k_2') for each substrate were obtained from plots of k_{obs} versus substrate concentration, and a plot of $\log(k_2')$ versus C−H bond strength is shown in Figure 2c. The linear relationship seen provides good support for the proposed mechanism involving a concerted HAT step as the rate-determining step.[47,48] Second-order kinetics for DHA and CHD were also obtained for $HBAr^{F}$ and also gave a linear correlation between $\log(k_2')$ and BDE(C−H) (Figure S14). Similar correlations with the BDE(C−H) of C−H substrates have been observed for both $Mn^{V}(O)(Cz)$ and $Fe^{IV}(O)(Cz^{\bullet+})$ species, implicating concerted HAT mechanisms.[46,49]

As reported by Abu-Omar, the corrole species $Mn^{IV}(OH)\text{-}(tpfc^{\bullet+})$, generated by addition of TFA to $Mn^{V}(O)(tpfc)$, is a close analog of $Mn^{IV}(O\text{-}LA)(TBP_8Cz^{\bullet+})$. It was concluded that the reactivity of the $Mn^{IV}(OH)(tpfc^{\bullet+})$ valence tautomer was strikingly different from the corrolazine analog, because of the stoichiometry of phenol oxidation and the lack of any rate enhancement in HAT compared to the $Mn^{V}(O)$ precursor. However, at the time of this study there was no information available on the corrolazine system with TFA as the Lewis acid. We examined the influence of TFA for the corrolazine case and found a remarkable

Author Manuscript Author Manuscript Author Manuscript Author Manuscript

similarity with the corrole results. The TFA adduct actually exhibits a slight deceleration in the rate of HAT for C−H bonds, as opposed to the other Lewis acids, all of which lead to rate enhancements. We speculate that there is little electronic effect on the HAT rate because TFA is such a weak Lewis acid, and the slight rate deceleration compared to the starting $Mn^{V}(O)$ may be due to a small steric inhibition from TFA. There does remain a significant difference in the stoichiometry of HAT between the corrolazine and the corrole complexes in the presence of TFA, with the Cz complex functioning as a one-electron oxidant, while the corrole complex functions as a two-electron oxidant. This difference suggests that the Mn^{IV} product following HAT is more stable in the Cz case.

The influence of Lewis acids on nonheme $M^{IV}(O)(N4Py)$ (M = Mn, Fe) has been investigated by Fukuzumi and Nam, and both rate accelerations and decelerations have been reported for C−H cleavage reactions.[18–20,50,51] Rate enhancements are observed if the driving force of electron transfer between the metal−oxo/Lewis acid adduct and the C−H substrate is reasonably favorable, as in the case of toluene derivatives as substrates.[18,51] For these substrates, the mechanism of C−H cleavage is described as proton-coupled electron transfer (PCET), where rate-limiting ET controls the kinetics and no KIE (i.e., KIE ≈ 1) for C−H/C−D is observed. In contrast, rate decelerations are observed when the redox potential of the substrate makes ET highly endergonic, such as for CHD.[19,20] A HAT mechanism is proposed for these substrates, and the lower reactivity is assigned to steric inhibition caused by the Lewis acid group.

For our corrolazine system, the data clearly point to a HAT mechanism, and steric inhibition is not a significant factor. The dominant influence over the reactivity is the strength of the Lewis acid, with stronger Lewis acids leading to much higher reaction rates for HAT by $Mn^{IV}(O\text{-}LA)(TBP_8Cz^{\bullet+})$ as compared to $Mn^{V}(O)(TBP_8Cz)$. Furthermore, the high-spin nature of the open-shell $Mn^{IV}(O\text{-}LA)(TBP_8Cz^{\bullet+})$ does not appear to be the source of the enhanced reactivity, because the TFA derivatives for both corrolazine and corrole show a decrease in HAT reaction rates. The reactivity of these heme-like metal−oxo Lewis acid adducts appear to be controlled by the strength of the Lewis acid.

SUMMARY AND CONCLUSIONS

We characterized the valence tautomer $Mn^{IV}(O\text{-}LA)\text{-}(TBP_8Cz^{\bullet+})$ by XAS, which confirmed the metal oxidation state is Mn^{IV} and showed that the Mn−O bond is elongated as compared to the $Mn^{V}(O)$ complex. The $Mn^{IV}(O\text{-}LA)\text{-}(TBP_8Cz^{\bullet+})$ complexes are able to cleave the C−H bonds in activated C−H substrates, and the reaction rates are dependent on C−H bond strength. These results, together with large KIEs, indicate C−H cleavage goes by an HAT mechanism. The strength of the Lewis acid in these complexes can change the rates of HAT by almost 30-fold. The change in electronic configuration for $Mn^{IV}(O\text{-}LA)(TBP_8Cz^{\bullet+})$ versus $Mn^{V}(O)\text{-}(TBP_8Cz)$ does not necessarily lead to enhanced reactivity of C−H cleavage, but rather the HAT reactivity appears to be dominated by the identity of the Lewis acid. These results suggest that careful tuning of high-valent metal−oxo reactivity in a heme protein environment could be controlled by appropriately timed proton delivery or H bonding to the metal−oxo unit.

Author Manuscript Author Manuscript Author Manuscript Author Manuscript

EXPERIMENTAL SECTION

Materials

The compound $Mn^{V}(O)(TBP_8Cz)$ was synthesized according to a published procedure.[24] All other reagents were commercially available and purchased at the highest level of purity and used as received unless otherwise specified here. The oxonium acid $HBAr^{F}$ ($[H(OEt_2)_2]^+[B(C_6F_5)_4]^-$) was synthesized according to a published procedure.[52] The substrate 9,10-dihydro-10-methylacridine ($AcrH_2$) was synthesized according to a published procedure.[41] The substrates xanthene (Xn) and 9,10-dihydroanthracene (DHA) were purchased from Sigma-Aldrich and recrystallized at least three times from ethanol. The substrate 1,4-cyclohexadiene (CHD) was purchased from Sigma-Aldrich and purified by running through an alumina pipette column immediately before use. The deuterated substrate xanthene-d_2 was synthesized according to a published procedure.[53] Deuterated solvents ($CDCl_3$ and CD_2Cl_2) for NMR were purchased from Cambridge Isotopes, Inc.

Instrumentation

UV−vis spectroscopy was performed on a Hewlett-Packard 8453 diode-array spectrophotometer equipped with HPChemstation software. A UV filter was used to block light <400 nm to protect the reaction mixtures from photoreduction. $^{31}P\{^1H\}$ NMR (161.9 MHz) spectra were recorded on a Bruker Avance 400 MHz NMR spectrometer at room temperature. Electron paramagnetic resonance (EPR) spectra were recorded with a Bruker EMX spectrometer equipped with a Bruker ER 041 X G microwave bridge and a continuous-flow liquid helium cryostat (ESR900) coupled to an Oxford Instruments TC503 temperature controller. The spectra were obtained at 12 K under nonsaturating microwave power conditions (microwave frequency = 9.43 GHz, microwave power = 20.1 mW, modulation amplitude = 10 G, modulation frequency = 100 kHz). Gas chromatography was performed on an Agilent 6850 gas chromatograph fitted with a DB-5 5% phenylmethyl siloxane capillary column and equipped with a flame-ionization detector (FID). The GC-FID response factor for anthracene was prepared versus eicosane as the internal standard. Stopped-flow experiments were carried out by using HiTech SHU-61SX2 (TgK scientific Ltd.) with a xenon light source and Kinetic Studio software. All calculations were performed using the Orca 3.0.3 program packages.[54] For computational convenience, all *tert*-butylphenyl groups on the TBP_8Cz ligand were replaced with H (H_8Cz). Unless specified, the resolution of identity (RI) approximation and the chain-of-sphere approximation (COSX), with the corresponding auxiliary basis sets, were applied to the Coulomb integrals on the DFT portion and exchange integrals on the Hartee-Fock (HF) portion, respectively, for hybrid functionals. The RI approximation was applied when pure functionals were used. LA = Lewis acids, which are $Zn(OTf)_2$ (with η^1, η^2 -$(OTf^-)_2$) and $B(C_6F_5)_3$.

X-ray Absorption Spectroscopy (XAS)

XAS data were recorded at the Stanford Synchrotron Radiation Laboratory (SSRL) on beamline 7–3 under ring conditions of 3 GeV and 495–500 mA. A Si(220), $\varphi = 90$, double-crystal monochromator was used for energy selection, and a Rh-coated mirror (set to an energy cutoff of 9.5 keV) was used for harmonic rejection. Energy calibration was performed by assigning the first inflection point of the Mn foil spectrum to 6539.0 eV. All

Author Manuscript Author Manuscript Author Manuscript Author Manuscript

samples were maintained at ~10 K during data collection using an Oxford Instruments CF1208 continuous-flow liquid helium cryostat. Data were measured in fluorescence mode (using a Canberra Ge element array detector). Samples were monitored for photo-reduction throughout the course of data collection. Only the scans which showed no evidence of photoreduction were used in the final data average.

The data were calibrated and averaged using EXAFSPAK. Pre-edge subtraction and splining were conducted using EXAFSPAK. A three-region cubic spline was used to model the smooth background above the edge. Normalization of the data was achieved by subtracting the spline and normalizing the postedge region to 1. The resultant EXAFS was k^3-weighted to enhance the impact of high-k data.

Theoretical EXAFS signals $c(k)$ were calculated using FEFF (version 7.0) and fit to the data using EXAFSPAK. The nonstructural parameter E_0 was also allowed to vary but was restricted to a common value for every component in a given fit. The structural parameters that were varied during the refinements were the bond distance (R) and the Debye–Waller factor, which is a measure of thermal vibration and to the static disorder of the absorbers and scatterers. Coordination numbers were systematically varied in the course of the analysis, but they were not allowed to vary within a given fit.

Formation of Mn^{IV}(O-LA)($TBP_8Cz^{\bullet+}$) for XAS

In a typical reaction, $Mn^{V}(O)(TBP_8Cz)$ (2 mM) was mixed with 1 equiv of Lewis acid ($Zn(OTf)_2$ or $B(C_6F_5)_3$) in benzonitrile. The reaction was monitored by UV−vis to ensure complete formation of Mn^{IV}(O-LA)($TBP_8Cz^{\bullet+}$) and transferred to a kapton XAS sample cell and carefully frozen in liquid nitrogen.

Analysis of the Reaction between Mn^{IV}(O-LA)($TBP_8Cz^{\bullet+}$) and C−H Substrates by EPR Spectroscopy

To an amount of $Mn^{V}(O)(TBP_8Cz)$ (1 mM) was added Lewis acid (1 equiv) (Zn(OTf)2, $B(C_6F_5)_3$, or $HBAr^F$), and a color change from green to brown was observed, indicating formation of Mn^{IV}(O-LA)-($TBP_8Cz^{\bullet+}$). Excess C−H substrate (100 equiv of either xanthene, DHA, or $AcrH_2$) was added, and the reaction was monitored by UV-vis until complete formation of the reduced Mn product was observed. This reaction mixture was then transferred to an EPR tube and frozen and stored at 77 K until EPR spectra could be recorded. The spectra were obtained at 12 K under nonsaturating microwave power conditions (microwave frequency = 9.43 GHz, microwave power = 20.1 mW, modulation amplitude = 10 G, modulation frequency = 100 kHz).

Product Analysis by GC-FID

To an amount of Mn^{V}(O)-(TBP_8Cz) (1.9 mM) in CH_2Cl_2 was added $B(C_6F_5)_3$ (1 equiv), and a color change from green to brown was observed indicating the formation of Mn^{V}(O-LA)($TBP_8Cz^{\bullet+}$). Excess DHA (100 equiv) in CH_2Cl_2 was added, and the reaction was monitored by UV−vis until complete formation of $Mn^{IV}(OH)(TBP_8Cz)$ was observed. Eicosane was added as an internal standard, and the mixture was injected onto the GC-FID for product analysis. The anthracene product was identified by comparison of retention time

Author Manuscript Author Manuscript Author Manuscript Author Manuscript

with an authentic sample, and quantitation was performed by integration of the peak and comparison with a calibration curve constructed with the internal standard. A yield of 65% (average of three runs) for the anthracene product was obtained.

Kinetics of Reaction between Mn^{IV}(O-LA)($TBP_8Cz^{\bullet+}$) and C−H Substrates

In a typical reaction, to an amount of Mn^{V}(O)-(TBP_8Cz) (64 μM) was added Lewis acid (1 equiv) (LA = TFA, $Zn(OTf)_2$, $B(C_6F_5)_3$, $HBAr^F$) in CH_2Cl_2, and the reaction was monitored by UV−vis until full formation of Mn^{IV}(O-LA)($TBP_8Cz^{\bullet+}$) was observed. Excess C−H substrate (Xn, DHA, or CHD) was added, and the spectrum for Mn^{IV}(O-$B(C_6F_5)_3$)($TBP_8Cz^{\bullet+}$) (λ_{max} = 420, 789 nm) was converted isosbestically to Mn^{IV}(X)(TBP_8Cz) (λ_{max} = 446, 722–727 nm). The pseudo-first-order rate constants, k_{obs}, for these reactions were obtained by nonlinear least-squares fitting of the plots of absorbances at 789 and 727 nm (Abs_t) versus time (t) according to the equation $Abs_t = Absf + (Abs_0 - Abs_f) \exp(-k_{obs}t)$, where Abs_0 and Abs_f are initial and final absorbance, respectively. The second-order rate constant was obtained from the slope of the best-fit line from a plot of k_{obs} versus substrate concentration and normalized per reactive C−H bond (k_2'). The reaction of Mn^{IV}(O-$B(C_6F_5)_3$)($TBP_8Cz^{\bullet+}$) with the C−H substrate $AcrH_2$ was too fast to be analyzed by conventional UV−vis kinetics and instead monitored by stopped-flow UV−vis spectroscopy. When $AcrH_2$ was added to Mn^{IV}(O-$B(C_6F_5)_3$)-($TBP_8Cz^{\bullet+}$), the spectrum changed to that of $Mn^{IV}(OH_2)$-(TBP_8CzH^+) (λ_{max} = 446, 727 nm). The rate constants were extracted as described earlier.

Lewis Acidity Measurements by the Gutmann-Beckett Method

A 3:1 mixture of Lewis acid ($HBAr^F$, TFA) and triethylphosphine oxide was prepared in CD_2Cl_2 and analyzed by $^{31}P\{^1H\}$ NMR spectroscopy. Spectra were collected and calibrated against an H_3PO_4 external standard. The following equation was used to calculate the acceptor number (A.N.): A.N. = $2.21(\delta_{sample} - 41.0)$, where δ_{sample} is the chemical shift for the $OPEt_3$−Lewis acid adduct.[44,45]

Geometry Optimization and Spin-State Ordering by DFT

Initial geometries for geometry optimization were obtained from the reported crystal structure for Mn^{V}(O)(TBP_8Cz).[28] Geometry optimization was performed using the unrestricted hybrid-GGA B3LYP[55] with dispersion correction (D3) from Grimme et al. in 2010.[56] The effective core potential basis set LANLDZ[57–61] was used for metal atoms, and 6–31G(d)[62,63] was used or the remaining atoms. Frequency calculations were performed on the optimized geometries, and no imaginary frequencies were observed. The Lewis acid complexes were examined in various spin states as follows: singlet ^{1}[Mn(O-LA)(H_8Cz)], triplet (ls-Mn^{IV}) ^{3}[Mn(O-LA)(H_8Cz)] (ls = low spin), triplet (hs-Mn^{IV}) ^{3}[Mn(O-LA)(H_8Cz)] (hs = high spin), and quintet ^{5}[Mn(O-LA)(H_8Cz)]. The triplet (ls-Mn^{IV}) ^{3}[Mn(O-LA)(H_8Cz)] has one unpaired spin on the Mn and one unpaired spin on the corrolazine with a $d_{\pi}^1 a''^1$ configuration. The other triplet state (hs-Mnn^{IV}) [Mn(O-LA)(H_8Cz)] has three unpaired spins on the Mn and an unpaired spin on the corrolazine ligand which is antiferromagnetically coupled.

Author Manuscript Author Manuscript Author Manuscript Author Manuscript

Single-point energy calculations on the optimized geometries were performed using range-separated hybrid meta-GGA wB97X with dispersion correction[56] (wB97X-D3) with def2-TZVPP on the metal atom and def2-SVP on the rest of the atoms. The zeroth-order regular approximation (ZORA) with a model potential[64] was applied along with segmented all-electron relativistically recontracted (SARC) version of the basis sets.[65,66] The RI approximation was applied to the Coulomb integral on the DFT portion, and the exchange integrals on the HF portion were solved exactly. Numerical grid was increased to "grid 4" in Orca notation, which is equal to Lebedev 302 points. Solvent was modeled by the conductor-like screening model (COSMO) with $\varepsilon = 9.08$ and refractive index = 1.424 for CH_2Cl_2.

Functional/Basis Set Benchmarking for the Geometry of Mn(O-B(C_6F_5)$_3$)(H_8Cz) by DFT

The initial geometry of Mn(O-B(C_6F_5)$_3$)(H_8Cz) for geometry optimizations was obtained from the reported crystal structure of Mn^V(O)(TBP_8Cz)[28] and the placement of a B(C_6F_5)$_3$ unit on the oxo ligand. Geometry optimizations were performed using the following combinations of functionals and basis sets: (1) BP86[67,68] and de2-ZVPP on Mn with def2-SVPD on the rest of the atoms. ZORA with a model potential[64] was applied, and the basis sets were recontracted (SARCs) [65,66] to be consistent with the ZORA. (2) B3PW91[68] with SDD[69] on Mn and 6–31G(d,p)[62,63] on the rest of the atoms. (3) B3LYP[55] with def2-TZVPP on Mn and def2-SVPD on the rest of the atoms. ZORA with a model potential[64] and SARCs[65,66] were applied. (4) B3LYP[55] with TZVPP on all atoms. ZORA with a model potential[64] and SARCs [65,66] were applied. (5) B3LYP[55] with LANLDZ[57–61] on Mn and 6–31G[62] on the rest of the atoms. (6) PBE0[70] with def2-TZVPP on Mn and def2-SVPD on the rest of the atoms. ZORA with a model potential[64] and SARCs[65,66] were applied.

Relaxed Surface Scans for Triplet (ls-Mn^{IV}) ^{3}[Mn(O-LA)-(H_8Cz)] and Quintet (hs-Mn^{IV}) ^{5}[Mn(O-LA)(H_8Cz)] by DFT

A similar procedure was used as for geometry optimization. Relaxed surface scans were performed with Mn−O distances varying from 1.61 to 1.71 Å with a fixed increment of 0.01 Å. Frequency calculations on the constrained geometries were not performed because the molecules were not fully relaxed. Single-point energies were calculated based on the constrained geometries using LANLDZ[57–61] on the metal atom and 6–31G(d)[62,63] on the rest of the atoms. For comparison, all single-point energies at different Mn−O distances were compared to that of the optimized ^{5}[Mn(O-LA)(H_8Cz)].

Supplementary Material

Refer to Web version on PubMed Central for supplementary material.

Acknowledgments

We thank the NIH for financial support (GM101153 to D.P.G.). RA.B. is grateful for the Harry and Cleio Greer Fellowship. We thank K. D. Karlin for access to the stopped-flow UV−vis spectrophotometer. Use of the Stanford Synchrotron Radiation Lightsource, SLAC National Accelerator Laboratory, is supported by the U.S. Department of Energy, Office of Science, Office of Basic Energy Sciences under Contract No. DE-AC02-76SF00515. The SSRL Structural Molecular Biology Program is supported by the DOE Office of Biological and Environmental Research, and by the National Institutes of Health, National Institute of General Medical Sciences (NIGMS). The

Author Manuscript Author Manuscript Author Manuscript Author Manuscript

contents of this publication are solely the responsibility of the authors and do not necessarily represent the official views of NIGMS or NIH (including P41GM103393).

REFERENCES

1. Rittle J, Green MT. Cytochrome P450 Compound I: Capture, Characterization, and C−H Bond Activation Kinetics. Science. 2010; 330:933–937. [PubMed: 21071661]
2. Denisov IG, Makris TM, Sligar SG, Schlichting I. Structure and chemistry of cytochrome P450. Chem. Rev. 2005; 105:2253–2278. [PubMed: 15941214]
3. Poulos TL. Heme Enzyme Structure and Function. Chem. Rev. 2014; 114:3919–3962. [PubMed: 24400737]
4. Weiss R, Bulach V, Gold A, Terner J, Trautwein AX. Valence-tautomerism in high-valent iron and manganese porphyrins. JBIC, J. Biol. Inorg. Chem. 2001; 6:831–845. [PubMed: 11713691]
5. Evangelio E, Ruiz-Molina D. Valence Tautomerism: New Challenges for Electroactive Ligands. Eur. J. Inorg. Chem. 2005; 2005:2957–2971.
6. Chirik PJ. Preface: Forum on Redox-Active Ligands. Inorg. Chem. 2011; 50:9737–9740. [PubMed: 21894966]
7. Leeladee P, Baglia RA, Prokop KA, Latifi R, de Visser SP, Goldberg DP. Valence Tautomerism in a High-Valent Manganese-Oxo Porphyrinoid Complex Induced by a Lewis Acid. J. Am. Chem. Soc. 2012; 134:10397–10400. [PubMed: 22667991]
8. Baglia RA, Dürr M, Ivanović-Burmazović I, Goldberg DP. Activation of a High-Valent Manganese-Oxo Complex by a Non-metallic Lewis Acid. Inorg. Chem. 2014; 53:5893–5895. [PubMed: 24873989]
9. Zaragoza JPT, Baglia RA, Siegler MA, Goldberg DP. Strong Inhibition of O-Atom Transfer Reactivity for Mn^{IV}(O)(π-Radical-Cation) (Lewis Acid) versus Mn^{V}(O) Porphyrinoid Complexes. J. Am. Chem. Soc. 2015; 137:6531–6540. [PubMed: 25964988]
10. Neu HM, Jung J, Baglia RA, Siegler MA, Ohkubo K, Fukuzumi S, Goldberg DP. Light-Driven, Proton-Controlled, Catalytic Aerobic C−H Oxidation Mediated by a Mn(III) Porphyrinoid Complex. J. Am. Chem. Soc. 2015; 137:4614–4617. [PubMed: 25839905]
11. Cong Z, Kurahashi T, Fujii H. Formation of Iron(III) meso-Chloro-isoporphyrin as a Reactive Chlorinating Agent from Oxoiron-(IV) Porphyrin π-Cation Radical. J. Am. Chem. Soc. 2012; 134:4469–4472. [PubMed: 22375905]
12. Boaz NC, Bell SR, Groves JT. Ferryl Protonation in Oxoiron(IV) Porphyrins and Its Role in Oxygen Transfer. J. Am. Chem. Soc. 2015; 137:2875–2885. [PubMed: 25651467]
13. Kurahashi T, Kikuchi A, Tosha T, Shiro Y, Kitagawa T, Fujii H. Transient Intermediates from Mn(salen) with Sterically Hindered Mesityl Groups: Interconversion between Mn^{IV}-Phenolate and Mn^{III}-Phenoxyl Radicals as an Origin for Unique Reactivity. Inorg. Chem. 2008; 47:1674–1686. [PubMed: 18237118]
14. Bougher CJ, Liu S, Hicks SD, Abu-Omar MM. Valence Tautomerization of High-Valent Manganese(V)-Oxo Corrole Induced by Protonation of the Oxo Ligand. J. Am. Chem. Soc. 2015; 137:14481–14487. [PubMed: 26517943]
15. Umena Y, Kawakami K, Shen J-R, Kamiya N. Crystal structure of oxygen-evolving photosystem II at a resolution of 1.9 Å. Nature. 2011; 473:55–60. [PubMed: 21499260]
16. Tsui EY, Tran R, Yano J, Agapie T. Redox-inactive metals modulate the reduction potential in heterometallic manganese-oxido clusters. Nat. Chem. 2013; 5:293–299. [PubMed: 23511417]
17. Suga M, Akita F, Hirata K, Ueno G, Murakami H, Nakajima Y, Shimizu T, Yamashita K, Yamamoto M, Ago H, Shen J-R. Native structure of photosystem II at 1.95 A resolution viewed by femtosecond X-ray pulses. Nature. 2015; 517:99–103. [PubMed: 25470056]
18. Park J, Morimoto Y, Lee Y-M, Nam W, Fukuzumi S. Unified View of Oxidative C−H Bond Cleavage and Sulfoxidation by a Nonheme Iron(IV)-Oxo Complex via Lewis Acid-Promoted Electron Transfer. Inorg. Chem. 2014; 53:3618–3628. [PubMed: 24605985]
19. Chen J, Lee Y-M, Davis KM, Wu X, Seo MS, Cho K-B, Yoon H, Park YJ, Fukuzumi S, Pushkar YN, Nam W. A Mononuclear Non-Heme Manganese(IV)-Oxo Complex Binding Redox-Inactive Metal Ions. J. Am. Chem. Soc. 2013; 135:6388–6391. [PubMed: 23324100]

Author Manuscript Author Manuscript Author Manuscript Author Manuscript

20. Chen J, Yoon H, Lee Y-M, Seo MS, Sarangi R, Fukuzumi S, Nam W. Tuning the reactivity of mononuclear nonheme manganese(iv)-oxo complexes by triflic acid. Chem. Sci. 2015; 6:3624–3632. [PubMed: 26146538]
21. Dong L, Wang Y, Lv Y, Chen Z, Mei F, Xiong H, Yin G. Lewis-Acid-Promoted Stoichiometric and Catalytic Oxidations by Manganese Complexes Having Cross-Bridged Cyclam Ligand: A Comprehensive Study. Inorg. Chem. 2013; 52:5418–5427. [PubMed: 23600453]
22. Lam WWY, Yiu S-M, Lee JMN, Yau SKY, Kwong H-K, Lau T-C, Liu D, Lin Z. BF_3-Activated Oxidation of Alkanes by MnO_4 . J. Am. Chem. Soc. 2006; 128:2851–2858. [PubMed: 16506763]
23. Cook SA, Borovik AS. Molecular Designs for Controlling the Local Environments around Metal Ions. Acc. Chem. Res. 2015; 48:2407–2414. [PubMed: 26181849]
24. Lansky DE, Mandimutsira B, Ramdhanie B, Clausen M, Penner-Hahn J, Zvyagin SA, Telser J, Krzystek J, Zhan R, Ou Z, Kadish KM, Zakharov L, Rheingold AL, Goldberg DP. Synthesis, Characterization, and Physicochemical Properties of Manganese(III) and Manganese(V)-Oxo Corrolazines. Inorg. Chem. 2005; 44:4485–4498. [PubMed: 15962955]
25. Neu HM, Quesne MG, Yang T, Prokop-Prigge KA, Lancaster KM, Donohoe J, DeBeer S, de Visser SP, Goldberg DP. Dramatic Influence of an Anionic Donor on the Oxygen-Atom Transfer Reactivity of a Mn^V-Oxo Complex. Chem. - Eur. J. 2014; 20:14584–14588. [PubMed: 25256417]
26. Charnock JM, Garner CD, Trautwein AX, Bill E, Winkler H, Ayougou K, Mandon D, Weiss R. Characterization of an Oxo(porphyrinato)manganese(IV) Complex by X-ray Absorption Spectroscopy. Angew. Chem., Int. Ed. Engl. 1995; 34:343–346.
27. Leto DF, Ingram R, Day VW, Jackson TA. Spectroscopic properties and reactivity of a mononuclear oxomanganese(iv) complex. Chem. Commun. 2013; 49:5378–5380.
28. Baglia RA, Prokop-Prigge KA, Neu HM, Siegler MA, Goldberg DP. Mn(V)(O) versus Cr(V)(O) Porphyrinoid Complexes: Structural Characterization and Implications for Basicity Controlling H-Atom Abstraction. J. Am. Chem. Soc. 2015; 137:10874–10877. [PubMed: 26295412]
29. Smeltz JL, Lilly CP, Boyle PD, Ison EA. The Electronic Nature of Terminal Oxo Ligands in Transition-Metal Complexes: Ambiphilic Reactivity of Oxorhenium Species. J. Am. Chem. Soc. 2013; 135:9433–9441. [PubMed: 23725588]
30. Yoon H, Lee Y-M, Wu X, Cho K-B, Sarangi R, Nam W, Fukuzumi S. Enhanced Electron-Transfer Reactivity of Nonheme Manganese(IV)-Oxo Complexes by Binding Scandium Ions. J. Am. Chem. Soc. 2013; 135:9186–9194. [PubMed: 23742163]
31. Peryshkov DV, Schrock RR, Takase MK, Muller P, Hoveyda AH. Z-Selective Olefin Metathesis Reactions Promoted by Tungsten Oxo Alkylidene Complexes. J. Am. Chem. Soc. 2011; 133:20754–20757. [PubMed: 22107254]
32. Barrado G, Doerrer L, Green MLH, Leech MA. Adducts of the Lewis acid $[B(C_6F_5)_3]$ with transition metal oxo compounds. J. Chem. Soc., Dalton Trans. 1999:1061–1066.
33. Scott MJ, Zhang HH, Lee SC, Hedman B, Hodgson KO, Holm RH. Oxygen-Bridged Iron-Copper Assemblies Pertinent to Heme-Copper Oxidases: Synthesis and Structure of an $[Fe^{III}$-(OH)-$Cu^{II}]$ Bridge and EXAFS Multiple-Scattering Effects of Linear Oxo and Nonlinear Hydroxo Bridges. J. Am. Chem. Soc. 1995; 117:568–569.
34. Fox S, Nanthakumar A, Wikstrom M, Karlin KD, Blackburn NJ. XAS Structural Comparisons of Reversibly Interconvertible Oxo- and Hydroxo-Bridged Heme-Copper Oxidase Model Compounds. J. Am. Chem. Soc. 1996; 118:24–34.
35. De Angelis F, Jin N, Car R, Groves JT. Electronic Structure and Reactivity of Isomeric Oxo-Mn(V) Porphyrins: Effects of Spin-State Crossing and pKa Modulation. Inorg. Chem. 2006; 45:4268–4276. [PubMed: 16676990]
36. de Visser SP, Ogliaro F, Gross Z, Shaik S. What Is the Difference between the Manganese Porphyrin and Corrole Analogues of Cytochrome P450's Compound I? Chem. - Eur. J. 2001; 7:4954–4960. [PubMed: 11763464]
37. Siegbahn PEM, Crabtree RH. Manganese Oxyl Radical Intermediates and O-O Bond Formation in Photosynthetic Oxygen Evolution and a Proposed Role for the Calcium Cofactor in Photosystem II. J. Am. Chem. Soc. 1999; 121:117–127.

Author Manuscript Author Manuscript Author Manuscript Author Manuscript

38. Ghosh A, Taylor PR. High-level ab initio calculations on the energetics of low-lying spin states of biologically relevant transition metal complexes: a first progress report. Curr. Opin. Chem. Biol. 2003; 7:113–124. [PubMed: 12547436]
39. Kropp H, King AE, Khusniyarov MM, Heinemann FW, Lancaster KM, DeBeer S, Bill E, Meyer K. Manganese Nitride Complexes in Oxidation States III, IV, and V: Synthesis and Electronic Structure. J. Am. Chem. Soc. 2012; 134:15538–15544. [PubMed: 22920682]
40. Ding M, Cutsail G III, Aravena D, Amoza M, Rouzieres M, Dechambenoit P, Losovyj Y, Pink M, Ruiz E, Clerac R, Smith JM. A Low Spin Manganese(IV) Nitride Single Molecule Magnet. Chem. Sci. 2016; 7:6132. [PubMed: 27746891]
41. Fukuzumi S, Kotani H, Prokop KA, Goldberg DP. Electron- and Hydride-Transfer Reactivity of an Isolable Manganese-(V)-Oxo Complex. J. Am. Chem. Soc. 2011; 133:1859–1869. [PubMed: 21218824]
42. Lansky DE, Goldberg DP. Hydrogen Atom Abstraction by a High-Valent Manganese(V)-Oxo Corrolazine. Inorg. Chem. 2006; 45:5119–5125. [PubMed: 16780334]
43. Joslin EE, Zaragoza JPT, Baglia RA, Siegler MA, Goldberg DP. The Influence of Peripheral Substituent Modification on P^{V}, Mn^{III}, and $Mn^{V}(O)$ Corrolazines: X-ray Crystallography, Electrochemical and Spectroscopic Properties, and HAT and OAT Reactivities. Inorg. Chem. 2016; 55:8646. [PubMed: 27529361]
44. Mayer U, Gutmann V, Gerger W. The acceptor number - A quantitative empirical parameter for the electrophilic properties of solvents. Monatsh. Chem. 1975; 106:1235–1257.
45. Beckett MA, Strickland GC, Holland JR, Sukumar Varma K. A convenient n.m.r. method for the measurement of Lewis acidity at boron centres: correlation of reaction rates of Lewis acid initiated epoxide polymerizations with Lewis acidity. Polymer. 1996; 37:4629–4631.
46. Prokop KA, de Visser SP, Goldberg DP. Unprecedented Rate Enhancements of Hydrogen-Atom Transfer to a Manganese(V)-Oxo Corrolazine Complex. Angew. Chem., Int. Ed. 2010; 49:5091–5095.
47. Warren JJ, Tronic TA, Mayer JM. Thermochemistry of proton-coupled electron transfer reagents and its implications. Chem. Rev. 2010; 110:6961–7001. [PubMed: 20925411]
48. Mayer JM. Understanding Hydrogen Atom Transfer: From Bond Strengths to Marcus Theory. Acc. Chem. Res. 2011; 44:36–46. [PubMed: 20977224]
49. Cho K, Leeladee P, McGown AJ, DeBeer S, Goldberg DP. A High-Valent Iron-Oxo Corrolazine Activates C−H Bonds via Hydrogen-Atom Transfer. J. Am. Chem. Soc. 2012; 134:7392–7399. [PubMed: 22489757]
50. Jung J, Kim S, Lee Y-M, Nam W, Fukuzumi S. Switchover of the Mechanism between Electron Transfer and Hydrogen-Atom Transfer for a Protonated Manganese(IV)-Oxo Complex by Changing Only the Reaction Temperature. Angew. Chem., Int. Ed. 2016; 55:7450.
51. Park J, Lee Y-M, Nam W, Fukuzumi S. Bronsted Acid-Promoted C−H Bond Cleavage via Electron Transfer from Toluene Derivatives to a Protonated Nonheme Iron(IV)-Oxo Complex with No Kinetic Isotope Effect. J. Am. Chem. Soc. 2013; 135:5052–5061. [PubMed: 23528016]
52. Jutzi P, Muller C, Stammler A, Stammler H-G. Synthesis, Crystal Structure, and Application of the Oxonium Acid $[H\text{-}(OEt_2)_2]^{+}[B(C_6F_5)_4]$. Organometallics. 2000; 19:1442–1444.
53. Goldsmith CR, Jonas RT, Stack TDP. C−H Bond Activation by a Ferric Methoxide Complex: Modeling the Rate-Determining Step in the Mechanism of Lipoxygenase. J. Am. Chem. Soc. 2002; 124:83–96. [PubMed: 11772065]
54. Neese F. The ORCA program system. Wiley Interdiscip. Rev.: Comput. Mol. Sci. 2012; 2:73–78.
55. Lee C, Yang W, Parr RG. Development of the Colle-Salvetti correlation-energy formula into a functional of the electron density. Phys. Rev. B: Condens. Matter Mater. Phys. 1988; 37:785–789.
56. Grimme S, Antony J, Ehrlich S, Krieg HA. consistent and accurate ab initio parametrization of density functional dispersion correction (DFT-D) for the 94 elements H-Pu. J. Chem. Phys. 2010; 132:154104. [PubMed: 20423165]
57. Hay PJ, Wadt WR. Ab initio effective core potentials for molecular calculations. Potentials for K to Au including the outermost core orbitals. J. Chem. Phys. 1985; 82:299–310.
58. Hay PJ, Wadt WR. Ab initio effective core potentials for molecular calculations. Potentials for the transition metal atoms Sc to Hg. J. Chem. Phys. 1985; 82:270–283.

Author Manuscript Author Manuscript Author Manuscript Author Manuscript

59. Feller D. The role of databases in support of computational chemistry calculations. J. Comput. Chem. 1996; 17:1571–1586.
60. Wadt WR, Hay PJ. Ab initio effective core potentials for molecular calculations. Potentials for main group elements Na to Bi. J. Chem. Phys. 1985; 82:284–298.
61. Schuchardt KL, Didier BT, Elsethagen T, Sun L, Gurumoorthi V, Chase J, Li J, Windus TL. Basis Set Exchange: A Community Database for Computational Sciences. J. Chem. Inf. Model. 2007; 47:1045–1052. [PubMed: 17428029]
62. Hehre WJ, Ditchfield R, Pople JA. Self-Consistent Molecular Orbital Methods. XII. Further Extensions of Gaussian-Type Basis Sets for Use in Molecular Orbital Studies of Organic Molecules. J. Chem. Phys. 1972; 56:2257–2261.
63. Hariharan PC, Pople JA. The influence of polarization functions on molecular orbital hydrogenation energies. Theor. Chim. Acta. 1973; 28:213–222.
64. van Wullen C. Molecular density functional calculations in the regular relativistic approximation: Method, application to coinage metal diatomics, hydrides, fluorides and chlorides, and comparison with first-order relativistic calculations. J. Chem. Phys. 1998; 109:392–399.
65. Pantazis DA, Chen X-Y, Landis CR, Neese F. All-Electron Scalar Relativistic Basis Sets for Third-Row Transition Metal Atoms. J. Chem. Theory Comput. 2008; 4:908–919. [PubMed: 26621232]
66. The Ahlrichs (2df,2pd) polarization functions were obtained from the TurboMole basis set library under ftp.chemie.unikarlsruhe.de/pub/basen
67. Perdew JP. Density-functional approximation for the correlation energy of the inhomogeneous electron gas. Phys. Rev. B: Condens. Matter Mater. Phys. 1986; 33:8822–8824.
68. Becke AD. Density-functional exchange-energy approximation with correct asymptotic behavior. Phys. Rev. A: At., Mol., Opt. Phys. 1988; 38:3098–3100.
69. Dolg M, Wedig U, Stoll H, Preuss H. Energy-adjusted ab initio pseudopotentials for the first row transition elements. J. Chem. Phys. 1987; 86:866–872.
70. Perdew JP, Burke K, Ernzerhof M. Generalized Gradient Approximation Made Simple. Phys. Rev. Lett. 1996; 77:3865–3868. [PubMed: 10062328]

Author Manuscript Author Manuscript Author Manuscript Author Manuscript

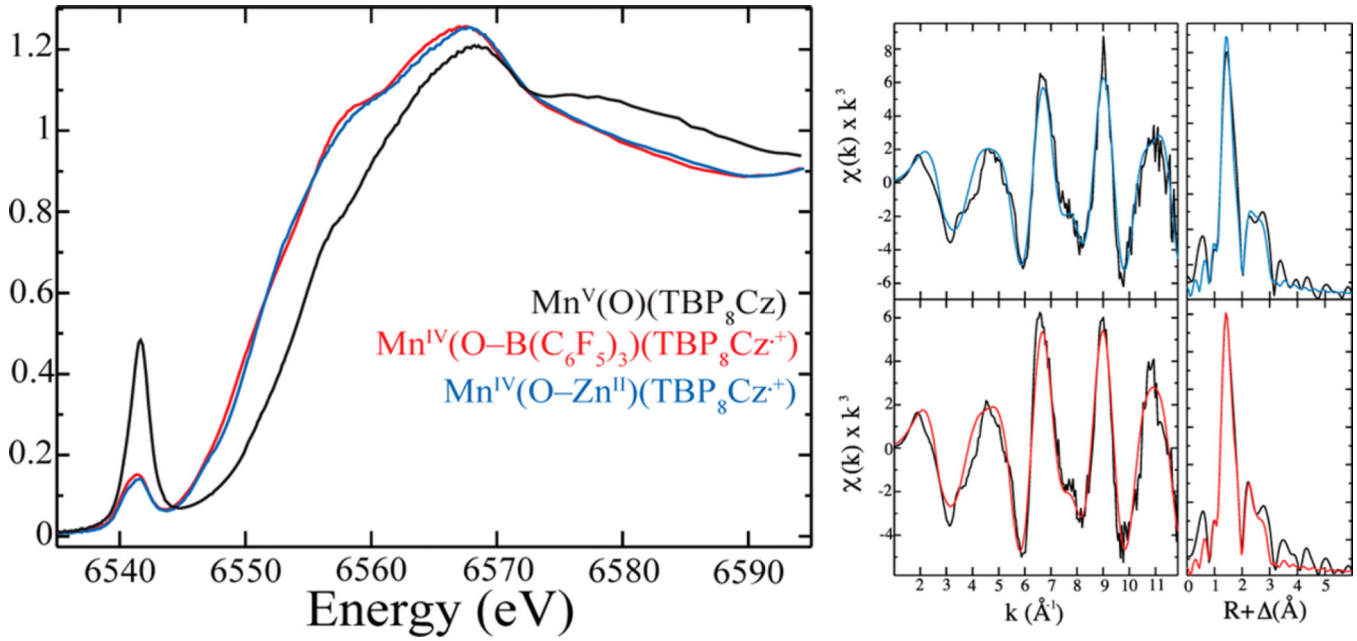

Figure 1.

(Left) Mn K-edge X-ray absorption spectra for $Mn^{V}(O)(TBP_8Cz)$ (black) and Mn^{IV}(O-LA)($TBP_8Cz^{\bullet+}$) (LA = $Zn(OTf)_2$ (blue) and $B(C_6F_5)_3$ (red)) in benzonitrile. (Right) EXAFS data of Mn^{IV}(O-LA)($TBP_8Cz^{\bullet+}$) (LA = $Zn(OTf)_2$ (blue) and $B(C_6F_5)_3$ (red)): data in black and best fits in color specified. Fit parameters of the best fits can be found in Table 1.

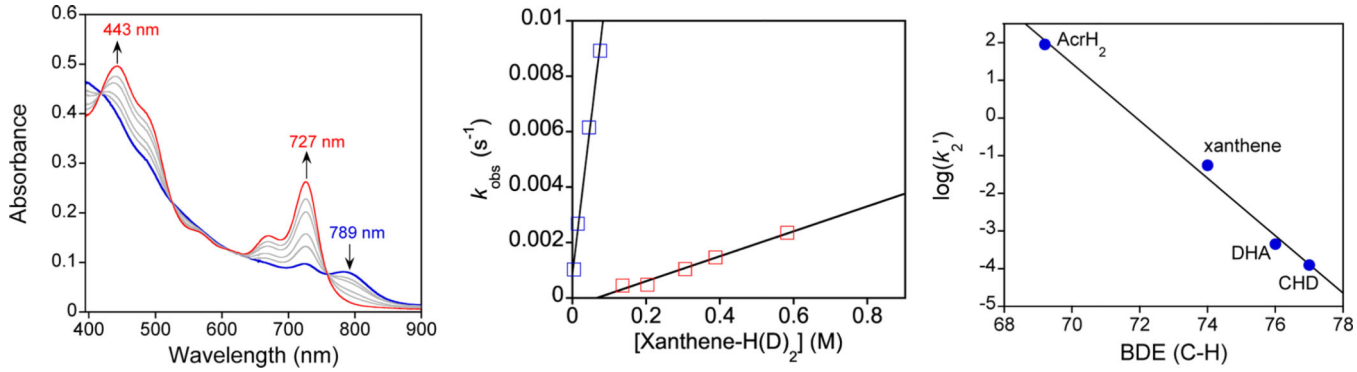

Figure 2.

(a) Time-resolved UV−vis spectra (0–30 min) for the reaction of $Mn^{IV}(O\text{-}B(C_6F_5)_3)(TBP_8Cz^{\bullet+})$ (14 μM) with excess xanthene in CH_2Cl_2 at 23 °C. (b) Second-order plots for xanthene (blue squares) and xanthene-d_2 (red squares) with $Mn^{IV}(O\text{-}B(C_6F_5)_3)(TBP_8Cz^{\bullet+})$. KIE = k_H/k_D = 25 ± 2. (c) Dependence of the log k values for $Mn^{IV}(O\text{-}B(C_6F_5)_3)(TBP_8Cz^{\bullet+})$ on the BDE values of the scissile C−H bond. Slope = −0.76 ± 0.05.

Author Manuscript Author Manuscript Author Manuscript Author Manuscript

Author Manuscript Author Manuscript Author Manuscript Author Manuscript

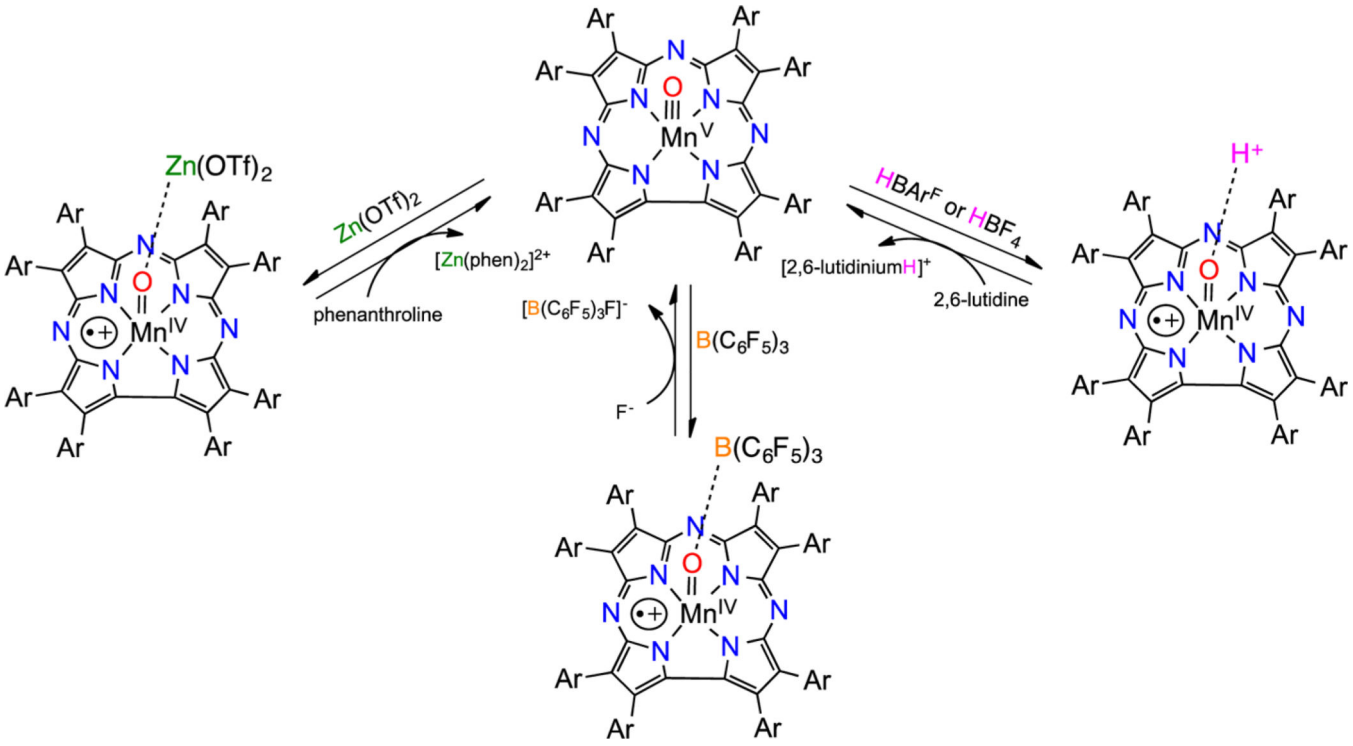

Scheme 1.

Reversible Binding of Lewis/Bronsted Acids Stabilizing Mn^{IV}(O-LA)($TBP_8Cz^{\bullet+}$) Complexes

Author Manuscript Author Manuscript Author Manuscript Author Manuscript

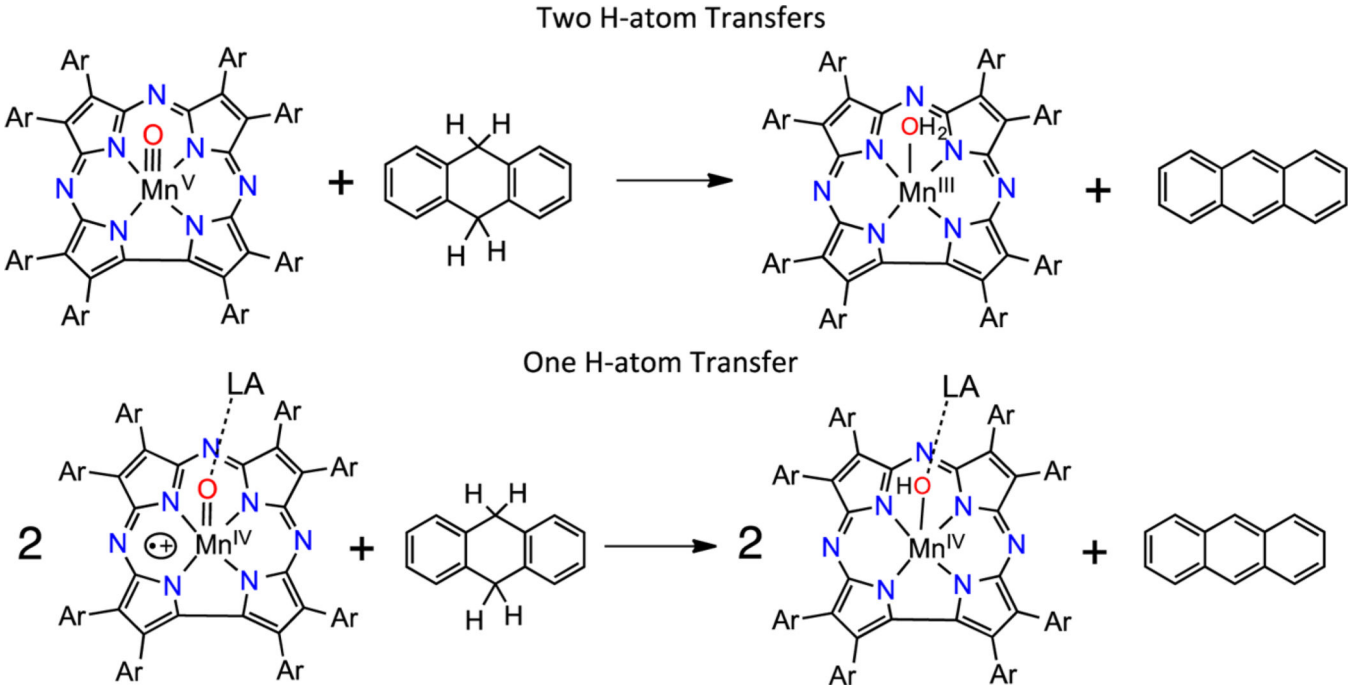

Scheme 2.

Comparison of Reaction Stoichiometries for $Mn^{V}(O)(TBP_8Cz)$ versus $Mn^{IV}(O\text{-}LA)(TBP_8Cz^{\bullet+})$

Author Manuscript Author Manuscript Author Manuscript Author Manuscript

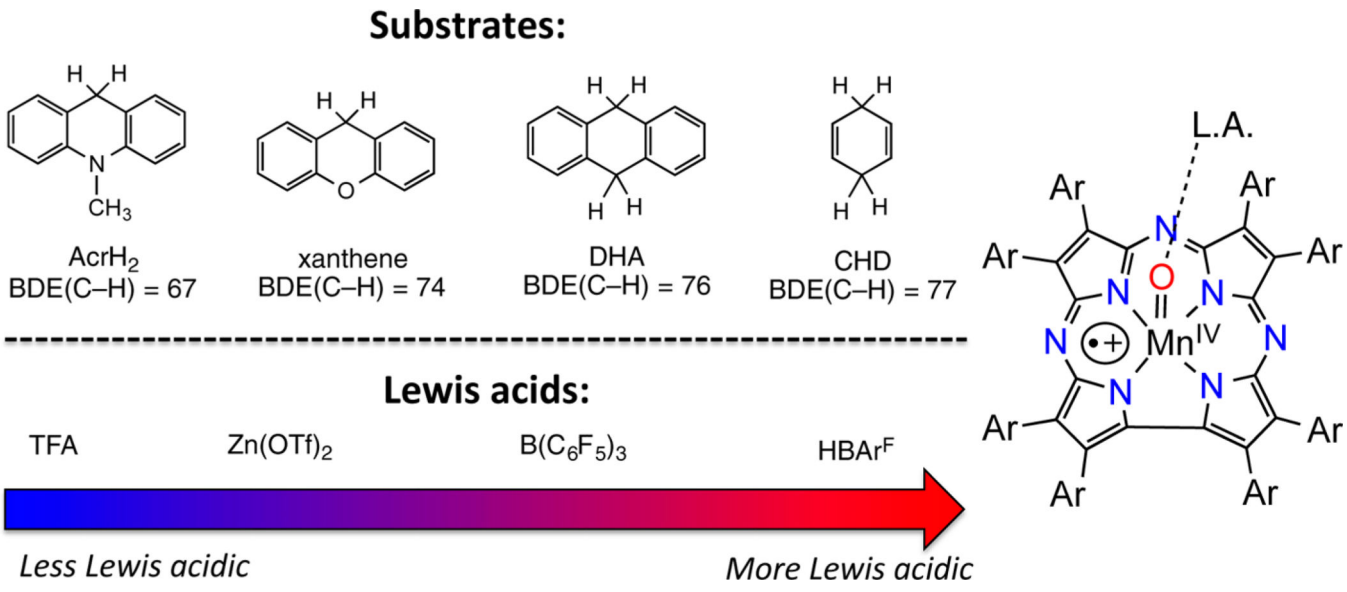

Chart 1.

Author Manuscript

Author Manuscript

Author Manuscript

Author Manuscript

Table 1

EXAFS Best-Fit Results for Mn^{IV}(O-LA)($TBP_8Cz^{\bullet+}$)

	LA = Zn^{2+}		LA = $B(C_6F_5)_3$	
	R **(Å)**	**σ (Å²)**	***R*** **(Å)**	**σ (Å²)**
1 Mn−O	1.61	0.0174	1.61	0.0167
4 Mn−N	1.89	0.00195	1.89	0.00223
16 Mn−N−C	3.12	0.00455	3.13	0.00981
8 Mn−C	2.90	0.00384	2.89	0.00551
ΔE_0	−5.28		−6.84	
error	0.312		0.295	

Author Manuscript

Author Manuscript

Author Manuscript

Author Manuscript

Table 2

Second-Order Rate Constants (k_2') (normalized per reactive C−H bond) for the Reaction of Mn^{IV}(O-LA)($TBP_8Cz^{\bullet+}$) with H-Atom Donor Substrates (units (k_2') = M^{-1} s^{-1})

Lewis acid (A.N.[a])	xanthene	k_{LA}/k_{none} (xanthene)	DHA[b]	CHD[c]
none[42,43]	$1.8 \pm 0.2 \times 10^{-3}$		$1.8 \pm 0.5 \times 10^{-5}$	$3.3 \pm 0.1 \times 10^{-5}$
TFA (40)	$9 \pm 1 \times 10^{-4}$	0.5		
$Zn(OTf)_2$ (68)	$8.1 \pm 0.4 \times 10^{-3}$	4		
$HBAr^F$ (102)	$1.9 \pm 0.2 \times 10^{-2}$	10	$6.7 \pm 0.1 \times 10^{-4}$	$2.0 \pm 0.1 \times 10^{-4}$
$B(C_6F_5)_3$ (82)	$5.5 \pm 0.3 \times 10^{-2}$	28	$4.3 \pm 0.2 \times 10^{-4}$	$1.3 \pm 0.8 \times 10^{-4}$

[a] A.N. = acceptor number.

[b] DHA = 9,10-dihydroanthracene.

[c] CHD = 1,4-cyclohexadiene.